IEEE Access
Multidisciplinary | Rapid Review | Open Access Journal

Received August 15, 2020, accepted September 13, 2020, date of publication September 18, 2020,
date of current version September 28, 2020.

Digital Object Identifier 10.1109/ACCESS.2020.3024638

Electromagnetic Vibration Analysis of Magnetically Controlled Reactor Considering DC Magnetic Flux

TONG BEN[1,3], (Member, IEEE), FANGYUAN CHEN[1,3], LONG CHEN[1,2,3], (Member, IEEE), AHMED ABU-SIADA[4], (Senior Member, IEEE), LIBING JING[1,3], (Associate Member, IEEE), AND RONGGE YAN[2]

[1]Hubei Provincial Engineering Technology Research Center for Power Transmission Line, China Three Gorges University, Yichang 443002, China
[2]State Key Laboratory of Reliability and Intelligence of Electrical Equipment, Hebei University of Technology, Tianjin 300130, China
[3]College of Electrical Engineering and New Energy, China Three Gorges University, Yichang 443002, China
[4]Discipline of Electrical and Computer Engineering, Curtin University, Perth, WA 6102, Australia

Corresponding author: Long Chen (chenlong@ctgu.edu.cn)

This work was supported in part by the National Natural Science Foundation of China under Grant 51777054, in part by the State Key Laboratory of Reliability and Intelligence of Electrical Equipment under Grant EERIKF2019009, in part by the Open Foundation of Hubei Provincial Engineering Technology Research Center for Power Transmission Line (China Three Gorges University) under Grant 2019KXL10, and in part by the Applied Basic Research Projects of Yichang under Grant A19-302-03.

ABSTRACT The main factors of stress distribution in MCRs are the magnetostriction effect of the core materials and the magnetic force between gaps under DC bias excitation. This article developed a coupling model for MCRs considering Maxwell magnetic force and magnetostriction under DC flux density biases. The constitutive equations of the magnetic field and strain field are constructed based on the magnetic property curves with a new measured and analyzed method to consider DC magnetic flux biases, which is the key contributions of this study. Then, the electromagnetic vibration properties of the MCR model are calculated and analyzed. To prove the validity of the proposed method, the vibration of a 4.4 kVar-220 V MCR is tested and analyzed.

INDEX TERMS Magnetically controlled reactors, finite element analysis, electromagnetic vibration, magnetostriction.

I. INTRODUCTION

High-Power magnetically controlled reactor (MCR) is a shunt static device that is widely used in high-voltage grids for the compensation of reactive power at the point of common coupling (PCC). By controlling the MCR core magnetization properties, rapid and smooth reactive power compensation at the PCC can be realized [1]. The main drawback of the MCRs is the significant mechanical vibration it exhibits because of the near magnetically saturated working conditions under AC and DC excitations, which result in low-frequency noise pollution, fastener loosening, and power grid faults [2], [3]. The noise due to such vibration is about 10 dB higher than the noise of traditional power transformers of the same capacity. Thus, the mechanical vibration of MCRs has become an issue that restricts its utilization at full capacity.

MCR mainly consists of AC power winding, the DC control winding, and the iron core. The AC power winding is connected to the PCC and produces alternating magnetic flux. The DC control winding is connected to a rectification circuit to generate a bias magnetic flux that offsets the main flux and controls the reactor to realize the reactive power regulation at the PCC [4]–[6]. The MCR adopts a sectionalized iron core structure with airgaps in which a non-magnetic conductive material is filled to limit the magnetic core saturation. Under the magnetic field strength provided by the power windings, the magnetic core is subjected to a Maxwell electromagnetic force [7], [8]. Meanwhile, the length and the volume of the ferromagnetic materials exhibit a slight change due to the core magnetization process. This phenomenon is referred as the magnetostrictive effect and magnetostrictive force. The magnetostrictive force is distorted in the airgap of the iron core when the magnetic field tends to saturate which signifies the electromagnetic vibration of the MCR [9]–[11]. To reduce the vibration and noise caused by the vibration

The associate editor coordinating the review of this manuscript and approving it for publication was Su Yan.

of the MCRs, the numerical models about simulating the electromagnetic force should be investigated, which will also be the basis for the optimization and design of the special structure motor [12], [13].

In recent years, several numerical models are proposed to calculate the electromagnetic vibration of the iron core. A magnetic-mechanical strong coupling finite element model to simulate the magnetostrictive vibration effect is proposed in [14]–[16]. Meanwhile, the stress caused by bending and cutting will affect the magnetostrictive properties, which leads to the magnetic flux concentrated and vibration and noise of the core more severely in this area [17]–[19]. However, the Maxwell electromagnetic force is not considered in this model. The Maxwell Stress Tensor (MST) method is used to investigate the radial force for PMBDC motors with 2-D FEM. And the vibration reduction scheme based on the above method has achieved good damping effect [20], [21]. An magnetostriction model considering the anisotropic magnetization properties based on backpropagation neural network is proposed in [22], [23] in which the vibration of a single-phase transformer is investigated. A numerical-based model for the static electromagnetic force is presented in [24] in which the correlation between the airgap length and the vertical displacement along with the influence of the Young's modulus on the vibration of the airgap filler material is investigated. The magnetostrictive orthogonal calculation method considering the magnetostrictive properties in different magnetization directions in [25], [26] is used to calculate the vibration characteristics of the cores of electrical equipment. The hysteresis magnetostriction characteristics of electrical steel is used to investigate the vibration and the noise of a transformer under different DC biases [27], [28].

While several analyzed methods have been introduced in the literature as discussed above, there are still many deficiencies in these methods when applied for electrical equipment, especially in the MCRs. For instance, the magnetic properties used to calculate the electromagnetic vibration in all presented studies were not measured under real operating conditions especially in DC bias flux magnetization conditions. When considering the DC and AC flux excitations, the MCR silicon steel materials are more likely to be magnetized to saturated corresponding to the magnetizing situation of the pure sinusoidal excitation [29]. Meanwhile, the DC magnetic flux density cannot be obtained using existing measuring methods, which results in inaccurate magnetic properties data and incorrect simulation results. Thus, the DC magnetic flux excitation must be simultaneously considered for accurate investigation of the electromagnetic vibration of the MCR which is the main contribution of this article.

This article proposes a numerical model coupling with electromagnetic force and mechanical characteristics for MCRs considering the DC magnetic flux bias of the silicon steels. Firstly, the magnetization curves and the magnetostrictive curves of silicon steel 30JG130 under AC with DC magnetic flux densities are measured. Secondly, based on the constitutive equation of the electromagnetic and mechanical fields, the numerical electromagneto-mechanical coupling three-dimensions (3D) MCR model of a 4.4 kVar-220 V MCR is constructed and analyzed. Finally, the MCR prototype is built and tested to prove the validity of the method proposed in this article.

II. ANALYSIS OF MAGNETIC PROPERTIES FOR MCR CORE

To accurately simulate the electromagnetic vibration of MCRs, the hysteresis loops and magnetization curves of electrical lamination under various magnetizing conditions should be measured and calculated as the material under different types of magnetizing conditions shows different saturated nonlinearity. As the MCR operation point is near magnetically saturated condition under AC with DC excitations, a new approach for measuring and analyzing the magnetic nonlinear properties of electrical steels under DC bias excitation is proposed below:

A. METHOD FOR ESTIMATING THE MAGNETIC CHARACTERISTIC OF SILICON LAMINATION WITH DC BIAS EXCITIZATION

Under the working conditions of MCRs, the alternating current in the AC power winding produces AC magnetic field H_{ac0} and AC flux density B_{ac0}. On the other hand, the direct current in the DC control winding produces DC magnetic field $H_{DC0.}$ and DC bias flux density ΔB. Thus, the theoretical AC and DC bias magnetization property of the lamination core comprises $B_{ac0} + \Delta B$ and $H_{ac0} + H_{DC0}$, as can be seen in Figure 1(a) and (c), respectively. The AC components B_{ac0} and H_{ac0} can be obtained by the B and the H measuring coils [30]. The DC components: H_{DC0} can be obtained using a magnetic circuit calculation method based on the applied DC current. However, ΔB cannot be measured or calculated directly. As a consequence, the practical magnetization property under DC field is represented by the AC bias magnetization property curve of B_{ac0} and $H_{ac0} + H_{DC0}$ (the blue curve in Figure 1(b)), which is not accurate to simulate the electromagnetic vibration properties of MCRs under working conditions. Thus, the key point to analyze the magnetization property of silicon steel is to obtain the DC magnetic flux biases under different AC magnetic flux densities.

This work proposes a new approach to obtain the DC bias magnetic flux density ΔB by changing the excitation forms in the measuring system. Firstly, H_{ac0} and H_{DC0} are applied in the measuring system and the AC bias magnetization curve of B_{ac0} and $H_{ac0} + H_{DC0}$ is obtained. Then, the AC magnetic field H_{ac1} with an equal amplitude of $H_{ac0} + H_{DC0}$ as shown in Figure 1(c) is applied and the produced magnetic flux density B_{ac1} is measured using B measuring coil. As a result, the second AC magnetization property curve of B_{ac1} and H_{ac1} (the black curve in Figure 1(b)) can be calculated. The DC magnetic flux density ΔB is calculated using the difference between the maximum values of B_{ac1} and B_{ac0}. Thus, by adding ΔB to B_{ac0}, theoretical AC, and DC bias magnetization property is obtained. Finally, based on this method families of the AC and DC bias magnetization curves

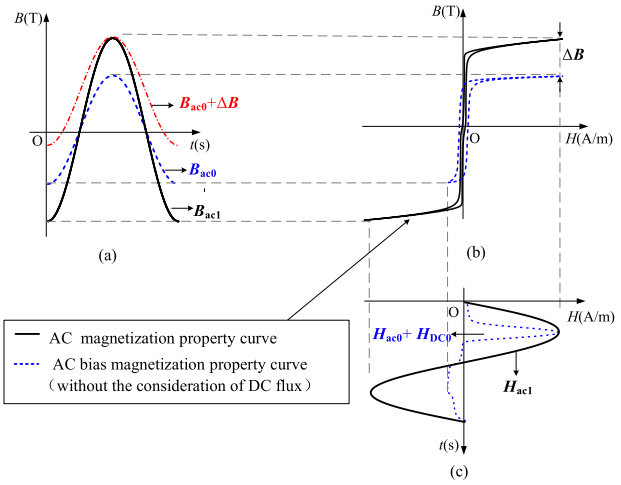

FIGURE 1. **Magnetic flux density and magnetic field waveforms with and without DC bias: (a) Magnetic flux density waveforms in the time domain, (b) The hysteresis loops of the material, (c) Magnetic field strength waveforms in the time domain.**

under a series of AC flux density levels can be measured and calculated.

The property of magnetostriction effect which is essential for the simulation of the electromagnetic vibration is the relationship between the magnetostriction λ and the magnetic field strength H. As the DC magnetic field can be obtained using magnetic circuit calculation based on the applied DC current, the magnetostrictive property curves can be obtained directly using the measuring system. As shown in Figure 2(b), the AC magnetostrictive property curve of H_{ac} and λ_{ac} is symmetrical to the λ- axis. The frequency of the magnetostriction curve of λ_{ac} shown in Figure 2(a) is two times the frequency of the excitation signal H_{ac}. Due to the saturated magnetization nonlinearity property under DC bias, the waveform of the magnetic strength field $H_{ac} + H_{DC}$ (red curves in Figure 2(c)) is sharp at the top area and

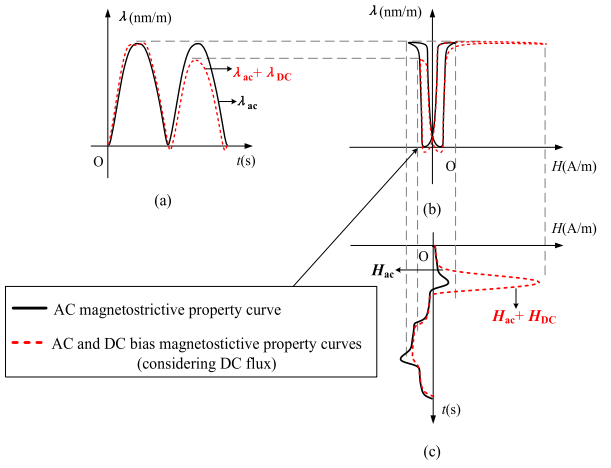

FIGURE 2. **Magnetostriction and magnetic field waveforms with and without DC bias: (a) Magnetostriction waveform in the time domain; (b) Magnetostrictive loops; (c) Magnetic field strength waveforms in the time domain.**

asymmetrical to the t-axis. Meanwhile, due to the saturated nonlinearity of magnetostriction property under DC bias, the waveform of magnetostriction (red curves in Figure 2(a)) shows two different peak points which lead to the fact that the frequency of the magnetostriction curve is the same as the excitation signal.

B. CHARACTERIZATION OF MAGNETIC AND MAGNETOSTRICTIVE PROPERTIES OF 30JG130 STEEL UNDER DC BIAS EXCITATION

The measuring system shown in Figure 3 is designed based on the standard IEC60404-3. The measuring device mainly includes an excitation system, sample support, an anti-vibration table, and a laser interferometer. The excitation system includes an external primary magnetization coil, an internal secondary measuring coil, and two magnetic yokes, which is supplied by a power amplifier with digital feedback control. The waveform output of the power amplifier is controlled by the NI PXI DAQ system which can provide arbitrary voltage waveforms in different service conditions. The magnetic circuit consists of two U-shape magnetic yokes and a test sample (600 mm∗100 mm). The magnetization coil is wound on the sample to be tested. The device is placed on an anti-vibration table to ensure the accuracy of laser emission and reception. Laser interferometer of resolution ratio 10 nm/m and working frequency 100 Hz emits a laser beam to the reflector. The deformation of the measured sample which is used to calculate the magnetostriction is obtained by calculating the time difference between the reflected and emitted laser beams.

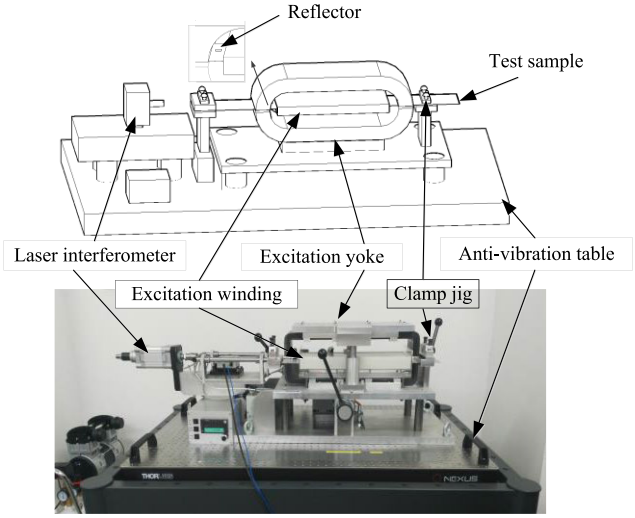

FIGURE 3. **Magnetization and magnetostriction measurement device.**

To obtain the magnetization curves and the magnetostriction curves of the material with the contribution of bias magnetic flux densities, the magnetic field and strain parameters under two kinds of excitations (B_{ac1} and H_{ac1}, B_{ac0} and $H_{ac0} + H_{DC0}$) are measured. Based on the method mentioned above, the measured hysteresis loops of the silicon steel sheet with different magnetic flux density levels under 80 A/m bias magnetic field are shown in Figure 4.

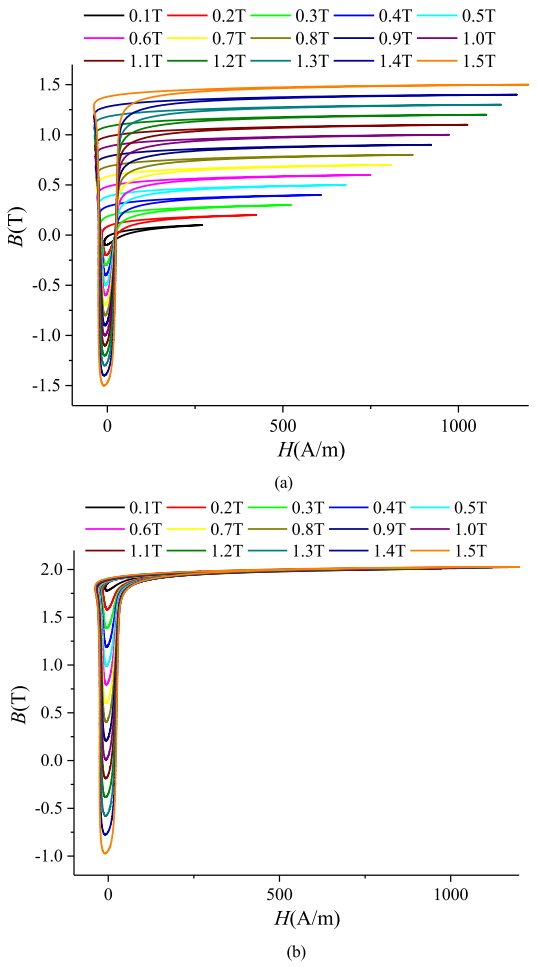

FIGURE 4. The measured hysteresis loops of silicon steel sheet with different magnetic flux density levels under 80 A/m bias magnetic field: (a) Without the consideration of DC magnetic flux; (b) Considering DC magnetic flux.

The hysteresis loops with lower flux density levels (0.1 T-1.4 T) shown in Figure 4(a) decreases gradually if the DC biases flux density is not considered, which means the magnetic flux density induced by the hysteresis loops in Figure 4(a) will be much lower than that in Figure 4(b) when the magnetic fields H are of the same values. The basic magnetization curves with and without DC magnetic flux density biases are plot by connecting the vertex points of the hysteresis loops which is shown in Figure 5. The permeability in Figure 5(a) is much lower than that in Figure 5(b) for specific magnetic field H. The magnetization curves without considering the DC magnetic flux biases ΔB are not appropriately used in the FEM calculation, which causes the reactor core to fail to reach the working magnetic flux density. Thus, the DC bias flux densities should be considered for accurate analysis.

As the DC bias field H_{DC} can be estimated indirectly by the Magnetization Current Method (MCM) and the magnetostrictive strain λ can be directly measured, the magnetostriction loops considering the DC bias field can be obtained as shown in Figure 6. The magnetostriction

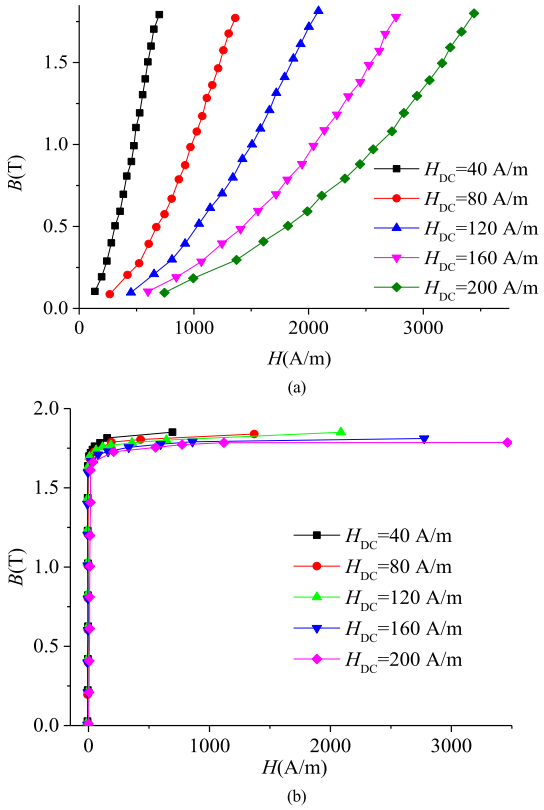

FIGURE 5. Magnetization curves with different ΔB: (a) Without the consideration of DC magnetic flux; (b) Considering DC magnetic flux.

property curves without DC bias excitation are symmetrical to the λ-axis, while it distorts when the DC bias is applied. Magnetostriction property curves with lower magnetic flux densities (0.1 T - 1.4 T) shown in Figure 6(b) decrease compared with the curves shown in Figure 6(a). It means that the strain which is resulted from the magnetostriction effect and based on the property of Figure 6(b) will be much lower than that of Figure 6(a). In the electromagnetic vibration simulation of electrical equipment, the magnetostriction single-value curve is enough to meet the requirement. Thus, the single-value curves of magnetostriction given in Figure 7 are obtained by connecting the vertex points on the magnetostriction loops with different working point. The single-value curves of magnetostriction gradually decrease with the increase of the DC bias magnetic fields.

The measured results show an obvious difference between the magnetization curves with and without considering the DC bias field, which is also true for magnetostriction properties of the material. So, the DC bias effect should be considered in the electromagnetic vibration computation of the MCR core.

III. MCR ELECTROMAGNETIC VIBRATION SIMULATION

A. ELECTROMAGNETO-MECHANICAL COUPLED CALCULATION 3D MODEL OF MCRS

The analyzed MCR is a three-limb core structure reactor shown in Figure 8. There are three airgaps in the middle of

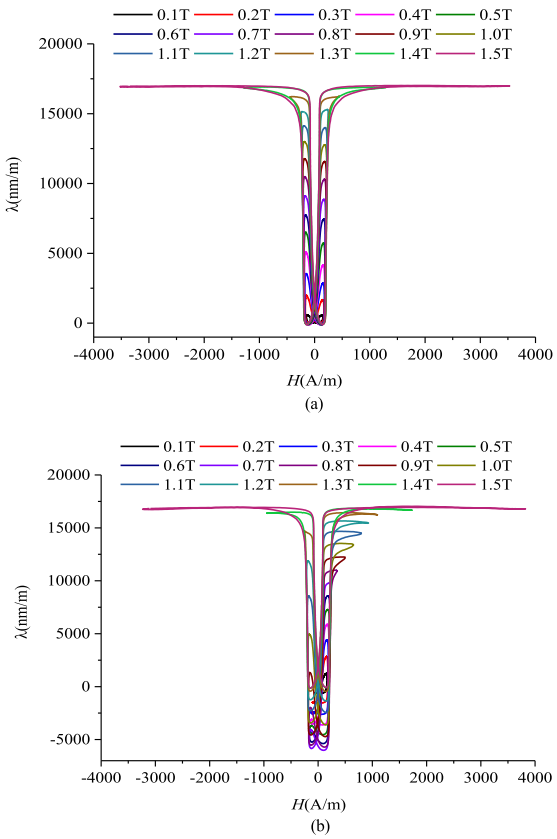

FIGURE 6. Magnetostrictive property curves under different bias magnetic fields: (a) Without DC bias excitation; (b) Considering DC magnetic flux.

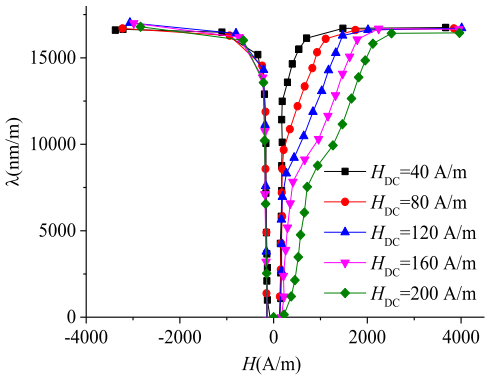

FIGURE 7. The single-value curves of magnetostriction of silicon steel sheet under different bias magnetic fields.

each core limb filled with a non-magnetic conductive material to reduce the magnetization saturation extent of the core. Two DC control windings are wrapped around the left and right core limbs, while the middle core limb is wrapped by the AC power coil.

To simulate the vibration of the magnetostriction effect with the DC magnetic flux density, the modified magnetization curves and magnetostrictive curves considering the DC bias effect proposed by out method is used. The relation matrix $\upsilon^{\mathbf{AC+DC}}$ between the magnetic flux density $\boldsymbol{B}$ and the

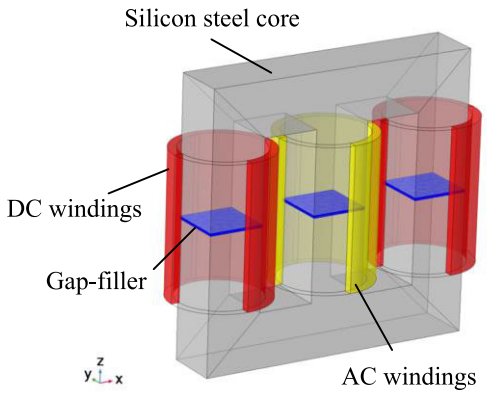

FIGURE 8. Structure of the MCR under investigation.

magnetic field strength $\boldsymbol{H}$, and the relation matrix $\boldsymbol{d}^{\mathbf{AC+DC}}$ between the magnetostriction strain $\varepsilon_{\mathbf{m}}$ and the magnetic field strength $\boldsymbol{H}$, are calculated. The constitutive relations of the magnetic field and magnetostrictive strain can be expressed as

$$\begin{cases} \boldsymbol{\varepsilon}_m = \boldsymbol{d}^{AC+DC}\boldsymbol{H} \\ \boldsymbol{H} = \boldsymbol{\upsilon}^{AC+DC}\boldsymbol{B} \end{cases} \tag{1}$$

where $\upsilon^{\mathbf{AC+DC}}$ and $\mathrm{d}^{\mathbf{AC+DC}}$ are the reluctivity matrix and magnetostrictive coefficient matrix, respectively. These are obtained from the measured magnetic properties data considering DC magnetic flux densities.

Equation (1) shows that the essence of magnetostriction is the energy exchange between the electromagnetic and mechanical systems. Based on the reference [9], the total energy function I(A, u) of the MCR core can be set. And the required solution is to find the optimum multi-function I(A, u) to minimize I(A, u) by using the energy variation principle.

The magnetostrictive energy $\boldsymbol{I}_{\mathbf{m}}$ is used to get the magnetostrictive force. According to the virtual work principle, the magnetostrictive force $\boldsymbol{f}_{\mathbf{m}}$ can be expressed as follows:

$$\begin{aligned} \boldsymbol{f}_{ms} &= -\frac{\partial \boldsymbol{I}_{ms}}{\partial \boldsymbol{u}} \\ &= \int_{\Omega_1} E\left(d_{11}^{AC+DC}\upsilon_{11}^{AC+DC}B_x\frac{\partial \varepsilon_x}{\partial u_x} + d_{22}^{AC+DC}\upsilon_{22}^{AC+DC}B_y \right. \\ &\quad \left. \times\frac{\partial \varepsilon_y}{\partial u_y} + d_{33}^{AC+DC}\upsilon_{22}^{AC+DC}B_z\frac{\partial \varepsilon_z}{\partial u_z}\right) dxdydz \end{aligned} \tag{2}$$

where E is the Young's Modulus.

Then, the pure elastic energy $\mathrm{I}_{\mathbf{e}}$ can be expressed as

$$\begin{aligned} \boldsymbol{I}_e &= \int_{\Omega_2}\frac{1}{2}\boldsymbol{\sigma}\cdot\boldsymbol{\varepsilon}d\boldsymbol{\Omega} \\ &= \int_{\Omega_2}\frac{E}{2(1+\alpha)}\left[\frac{\alpha}{1-2\alpha}\left(\varepsilon_x+\varepsilon_y+\varepsilon_z\right)^2 \right. \\ &\quad \left. +\varepsilon_x^2+\varepsilon_y^2+\varepsilon_z^2+\frac{1}{2}\left(\gamma_{xy}^2+\gamma_{yz}^2+\gamma_{zx}^2\right)\right]\mathrm{d}x\mathrm{d}y\mathrm{d}z \end{aligned} \tag{3}$$

where α is the Poisson Ratio.

TABLE 1. Material parameters values of MCR model.

	Relative permeability (1)	Poisson Ratio (1)	Young's Modulus (GPa)
Gap Filler (Epoxide resin)	1	0.38	1
Silicon Steel Core (30JG130)	–	0.31	110
Windings (copper)	1	0.35	110

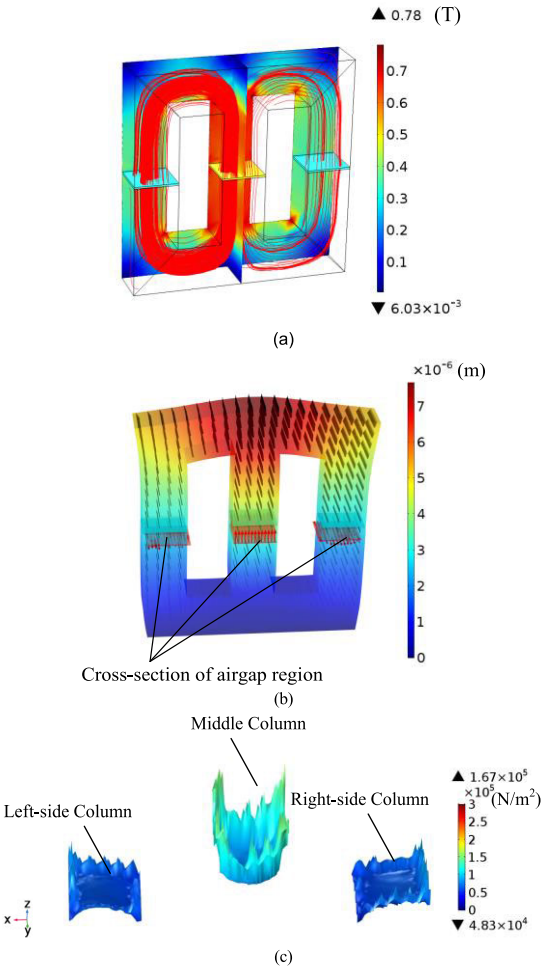

FIGURE 9. The simulation results of MCR core at $t = 0.015$ s under the bias magnetic fields of 40 A/m: (a) Magnetic flux density; (b) Displacement; (c) Stress.

The magnetic stress can be expressed as:

$$f_{mw} = \int_S \begin{bmatrix} B_xH_x - \frac{1}{2}BH & B_xH_y & B_xH_z \\ B_yH_x & B_yH_y - \frac{1}{2}BH & B_yH_z \\ B_zH_x & B_zH_y & B_zH_z - \frac{1}{2}BH \end{bmatrix} \times \begin{bmatrix} n_x \\ n_y \\ n_z \end{bmatrix} \mathrm{d}S \quad (4)$$

B. SIMULATION RESULTS OF MCR

Based on the proposed model of MCR, the electromagnetic vibration characteristics can be calculated. A fixed constraint

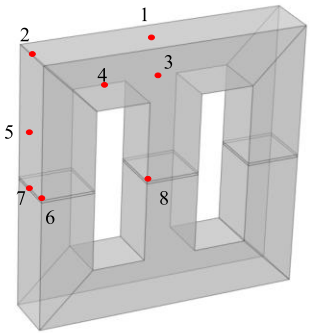

FIGURE 10. The distribution position of the points.

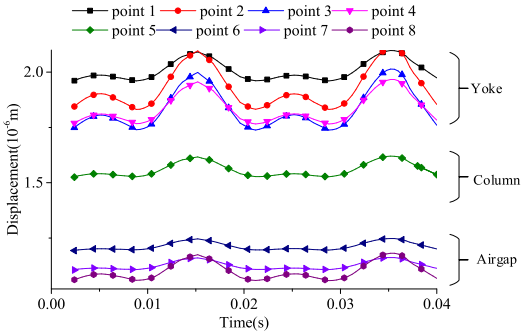

FIGURE 11. The displacement curves in points 1-8 of MCR core under the bias magnetic fields of 40 A/m.

condition was added to the model to simulate the actual working situation. The material parameters values of MCR model are shown in table 1. The nonlinear relative permeability of silicon steel core is calculated based on magnetization curves in Figure 5(b). The other material parameters values in table 1 are acquire from the database of JFE Steel Corporation [30].

By applying an excitation voltage of 200 V, 50 Hz to the AC power winding, and different DC currents to the DC control windings, the magnetic field strength and displacement distribution of the MCR cores are computed. The maximum displacement of the MCR core is 7×10^{-6} m when the maximum magnetic flux density reaches 0.78 T as shown in Figure 9. The stress is concentrated on four corners of the middle column, the center of the left-side column and the right-side column.

To study the vibration characteristic at some key areas of the MCR core as shown in Figure 10, the displacement curves at points 1-8 with times are analyzed as shown in Figure 11. As shown, the most obvious deformation positions are located at points 1-4 on the yoke of the MCR core while the least obvious deformation positions are located at points 6-8 that are in the airgap. To obtain the influence of the measured magnetic properties on the vibration displacement, the displacements and magnetic field strength waveform in the time domain at point 6 and point 8 are compared. From Figure 12, we can get the period of the displacement waveform is the same as the magnetic field waveform, which is the same trend of the magnetostriction curves shown in Figure 2(a). Thus,

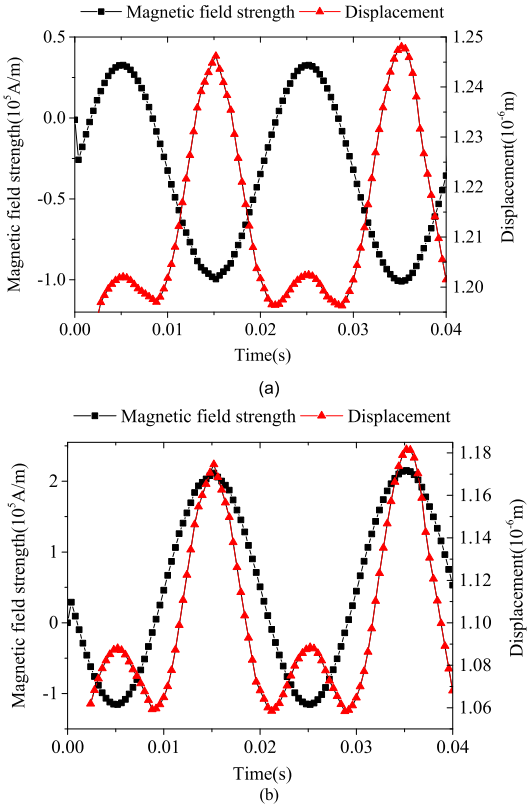

FIGURE 12. The comparison of magnetic field strength and displacement in point 6 and point 8 of MCR core under the bias magnetic fields of 40 A/m: (a) Point 6; (b) Point 8.

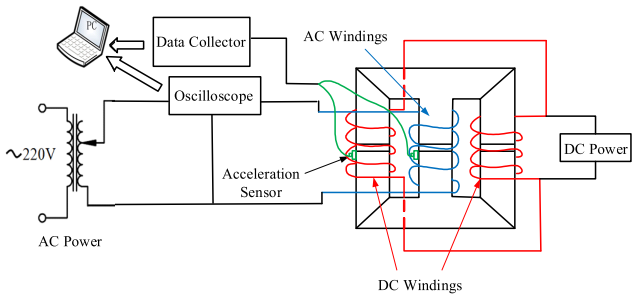

FIGURE 13. Schematic diagram of the vibration test system for MCR.

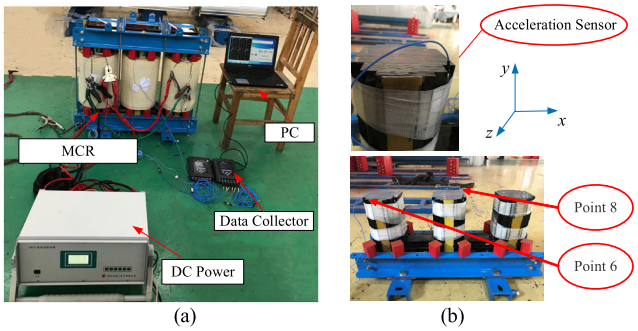

FIGURE 14. The vibration test system for MCR prototype: (a) MCR prototype test system; (b) position of the acceleration sensors.

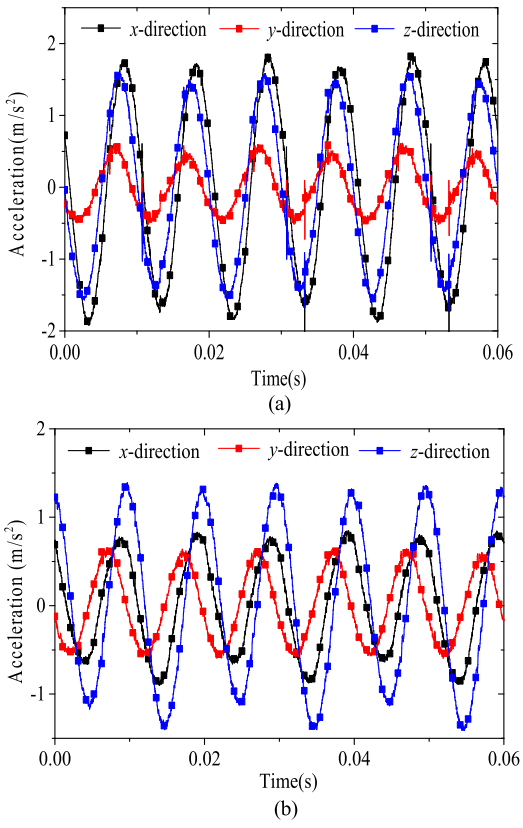

FIGURE 15. The acceleration curves of the core around the airgap when $I_{DC} = 0$ A: (a) point 6; (b) point 8.

the magnetostriction effect is the most important factor of the MCR core vibration under DC bias excitation.

IV. THE VERIFICATION EXPERIMENT OF MCRS MODEL

A. MCR VIBRATION TEST

The schematic diagram of the developed vibration test system for MCR is shown in Figure 13. In addition to the magnetostriction effect, Maxwell electromagnetic force which is generated in the airgap region is also one of the main sources of vibration. Thus, the acceleration sensors are set on the MCR cores in the vicinity of the airgap area to analyze the key sources of vibration. The AC and DC coils, airgap gasket, fixture, and other components are assembled as shown in the hardware setup in Figure 14. The vibration test system including the Data collector (model: SQuadriga), acceleration sensor (model: 352C23, serial: LW172875, sensitivity:0.529mV/m/s^2) and PC. Parameters of the MCR test in this article are shown in table 2.

The size of the tested reactor core is consistent with the calculation model, and the material used in core is 30JG130 silicon steel, which is the same grade used in the model. The AC winding and the DC magnetomotive force are consistent with the simulation model. In the case of an equal DC magnetomotive force in the simulation and the experiment, the control DC current I_{DC} is set at 5 A according to the Ampere circuital

TABLE 2. Parameters of the MCR.

Type of MCR	EKDG-4.4kVar-220V
Rated frequency (Hz)	50
AC rated voltage (V)	220
AC winding turns	234

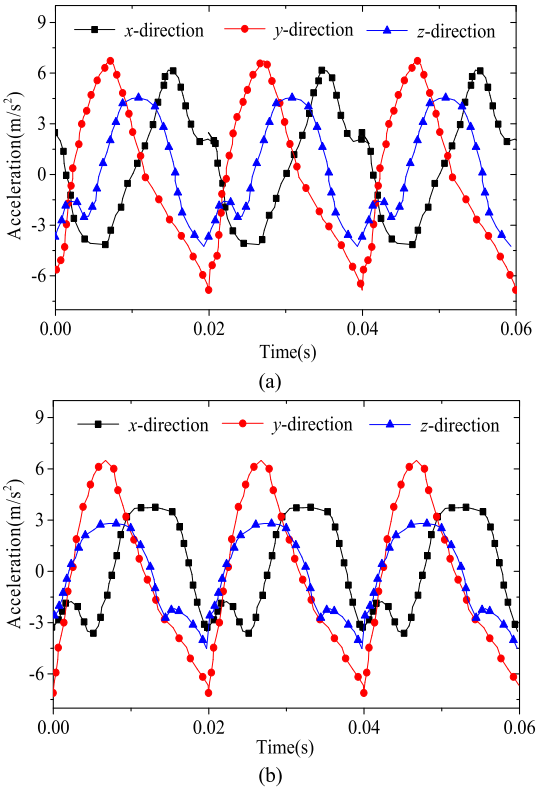

FIGURE 16. The acceleration curves of the core around the airgap when $I_{DC} = 5$ A: (a) point 6; (b) point 8.

theorem, when the magnetic field in the simulation model is 160 A/m. The measured acceleration of the core around the airgap (points 6 and 8) when $I_{DC} = 0$ A and $I_{DC} = 5$ A are shown in Figures 15 and 16, respectively.

As shown in Figures. 15 and 16, the waveforms of the acceleration in all three directions are sinusoidal when $I_{DC} = 0$ A, while the waveforms are sharp at the top and bottom areas when $I_{DC} = 5$ A. Also, it can be observed that the amplitude of the acceleration curves at point 6 is larger than that at point 8, which agrees with the obtained simulation results. The vibration cycles when $I_{DC} = 0$ A and $I_{DC} = 5$ A are 0.01 s and 0.02 s, respectively, which is in the same trend as the magnetostriction curves in Figure 2(a). This change of the vibration cycles is due to the saturated nonlinearity of the magnetostriction properties under DC bias magnetization and the asymmetry of the magnetic strength field to the time axis.

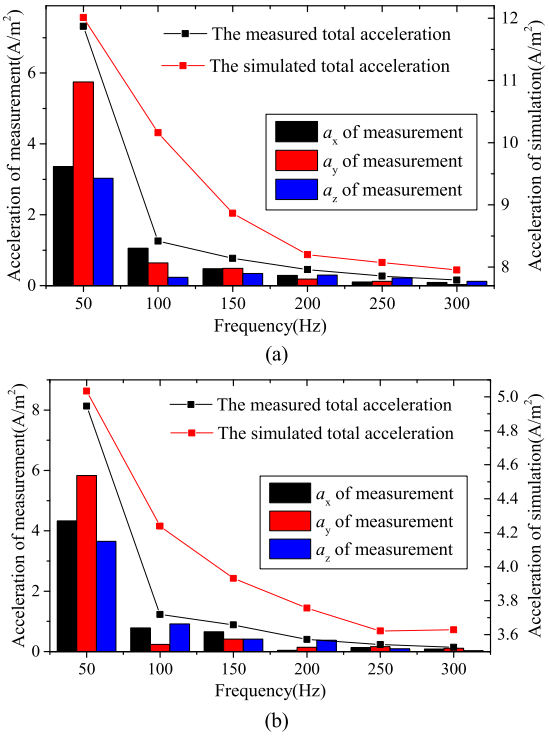

FIGURE 17. Comparison between the experimental and simulated results under DC bias: (a) point 6; (b) point 8.

B. COMPARISON OF EXPERIMENTAL AND SIMULATED RESULTS

To verify the proposed method in this article, the frequency characteristics of the vibration accelerations are compared between the experimental and numerical results. The measured total accelerations can be obtained from:

$$a = \sqrt{a_x^2 + a_y^2 + a_z^2} \tag{5}$$

where a_x, a_y, a_z are the accelerations in x, y, and z directions, respectively.

As shown in Figure 17, the acceleration is in the low-frequency range and at 50Hz is the most dominant component. Due to several stochastic factors such as mechanical components, harmonic, lamination and joint of iron core in addition to electromagnetic vibration, which cannot be accurately simulated in the MCR model, the simulation results are not completely consistent with the experimental data. However, the difference between the measurement and the simulation data is within reasonable accepted limits.

V. CONCLUSION

This article studies the electromagnetic vibration properties of MCR with a focus on the influence of DC bias magnetic flux. By using the AC and DC bias magnetization and magnetostriction curves of the 30JG130 steel sheet, an accurate vibration analyzing model of MCR can be provided. Results show that two peak points appear during one vibration cycle and the vibrations in the middle limb (wound by AC power winding) and the two-side limbs (wound by DC control

windings) are not synchronized. Meanwhile, the amplitude and frequency of the measured vibration accelerations based on the MCR prototype test are in the same trend with the simulated results, which verify the validity of the proposed method.

REFERENCES

[1] M. Tümay, T. Demirdelen, S. Bal, R. İ. Kayaalp, B. Doğru, and M. Aksoy, "A review of magnetically controlled shunt reactor for power quality improvement with renewable energy applications," *Renew. Sustain. Energy Rev.*, vol. 77, pp. 215–228, Sep. 2017.

[2] K.-Y. Yoo, B. K. Lee, and D.-H. Kim, "Investigation of vibration and acoustic noise emission of powder core inductors," *IEEE Trans. Power Electron.*, vol. 34, no. 4, pp. 3633–3645, Apr. 2019.

[3] A. Murat, S. Sokolov, A. Saukhimov, and A. Dolgopolov, "Research and modeling of magnetically controlled shunt reactors in PSCAD/EMTDC," in *Proc. 7th Int. Conf. Electr. Electron. Eng. (ICEEE)*, Antalya, Turkey, Apr. 2020, pp. 155–159.

[4] Y. Terriche, C.-L. Su, M. U. Mutarraf, M. Mehrzadi, A. Lashab, J. M. Guerrero, and J. C. Vasquez, "Harmonics mitigation in hybrid AC/DC shipboard microgrids using fixed capacitor-thyristor controlled reactors," in *Proc. IEEE Int. Conf. Environ. Electr. Eng., IEEE Ind. Commercial Power Syst. Eur. (EEEIC/I CPS Eur.)*, Madrid, Spain, Jun. 2020, pp. 1–6.

[5] M. Tian, J. Li, P. Shi, and Y. Guo, "A novel quickness improvement method of a magnetic-valve controllable reactor," *IEEE Trans. Appl. Supercond.*, vol. 26, no. 7, pp. 1–5, Oct. 2016.

[6] S. Rahmani, A. Hamadi, K. Al-Haddad, and L. A. Dessaint, "A combination of shunt hybrid power filter and thyristor-controlled reactor for power quality," *IEEE Trans. Ind. Electron.*, vol. 61, no. 5, pp. 2152–2164, May 2014.

[7] J. Avila-Montes, D. Campos-Gaona, E. M. Vázquez, and J. R. Rodríguez-Rodríguez, "A novel compensation scheme based on a virtual air gap variable reactor for AC voltage control," *IEEE Trans. Ind. Electron.*, vol. 61, no. 12, pp. 6547–6555, Dec. 2014.

[8] M. K. Ghosh, Y. Gao, H. Dozono, K. Muramatsu, W. Guan, J. Yuan, C. Tian, and B. Chen, "Proposal of maxwell stress tensor for local force calculation in magnetic body," *IEEE Trans. Magn.*, vol. 54, no. 11, Nov. 2018, Art. no. 7206204.

[9] A. Lotfi and M. Faridi, "Design optimization of gapped-core shunt reactors," *IEEE Trans. Magn.*, vol. 48, no. 4, pp. 1673–1676, Apr. 2012.

[10] B. Tong, Y. Qingxin, Y. Rongge, Z. Lihua, and Z. Changgeng, "Research on stress characteristics of shunt reactor considering magnetization and magnetostrictive anisotropy," *IEEE Trans. Magn.*, vol. 54, no. 3, pp. 1–4, Mar. 2018.

[11] T. Tanzer, H. Pregartner, M. Riedenbauer, R. Labinsky, M. Witlatschil, A. Muetze, and K. Krischan, "Magnetostriction of electrical steel and its relation to the no-load noise of power transformers," *IEEE Trans. Ind. Appl.*, vol. 54, no. 5, pp. 4306–4314, Sep. 2018.

[12] L. Jing, Z. Huang, J. Chen, and R. Qu, "An asymmetric pole coaxial magnetic gear with unequal Halbach arrays and spoke structure," *IEEE Trans. Appl. Supercond.*, vol. 30, no. 4, pp. 1–5, Jun. 2020.

[13] A. Shahaj and S. D. Garvey, "A possible method for magnetostrictive reduction of vibration in large electrical machines," *IEEE Trans. Magn.*, vol. 47, no. 2, pp. 374–385, Feb. 2011.

[14] L. Zhu, Y. Li, Y. Yang, Q. Yang, and X. Zhang, "Electromagnetic vibration of controllable saturable reactor under different DC control current," *Int. J. Appl. Electromagn. Mech.*, vol. 55, pp. 217–227, Oct. 2017.

[15] W. Kitagawa, Y. Ishihara, T. Todaka, and A. Nakasaka, "Analysis of structural deformation and vibration of a transformer core by using magnetic property of magnetostriction," *Electr. Eng. Jpn.*, vol. 172, no. 1, pp. 19–26, Jul. 2010.

[16] C. A. Baguley, U. K. Madawala, and B. Carsten, "The impact of vibration due to magnetostriction on the core losses of ferrite toroidals under DC bias," *IEEE Trans. Magn.*, vol. 47, no. 8, pp. 2022–2028, Aug. 2011.

[17] P. K. Klimczyk, P. Anderson, A. Moses, and M. Davies, "Influence of cutting techniques on magnetostriction under stress of grain oriented electrical steel," *IEEE Trans. Magn.*, vol. 48, no. 4, pp. 1417–1420, Apr. 2012.

[18] P. I. Anderson, A. J. Moses, and H. J. Stanbury, "Assessment of the stress sensitivity of magnetostriction in grain-oriented silicon steel," *IEEE Trans. Magn.*, vol. 43, no. 8, pp. 3467–3476, Aug. 2007.

[19] Y.-H. Chang, C.-H. Hsu, H.-L. Chu, and C.-P. Tseng, "Magnetomechanical vibrations of three-phase three-leg transformer with different amorphous-cored structures," *IEEE Trans. Magn.*, vol. 47, no. 10, pp. 2780–2783, Oct. 2011.

[20] S. Wang, J. Hong, Y. Sun, and H. Cao, "Analysis and reduction of electromagnetic vibration of PM brush DC motors," *IEEE Trans. Ind. Appl.*, vol. 55, no. 5, pp. 4605–4612, Sep. 2019.

[21] S. Wang, J. Hong, Y. Sun, and H. Cao, "Analysis of zeroth-mode slot frequency vibration of integer slot permanent-magnet synchronous motors," *IEEE Trans. Ind. Electron.*, vol. 67, no. 4, pp. 2954–2964, Apr. 2020.

[22] S. A. Ansari, M. Haroon, Z. Sheikh, and Z. Kazmi, "Detection of flow-induced vibration of reactor internals by neutron noise analysis," *IEEE Trans. Nucl. Sci.*, vol. 55, no. 3, pp. 1670–1677, Jun. 2008.

[23] Z. Wang, Y. Zhang, Z. Ren, C.-S. Koh, and O. A. Mohammed, "Modeling of anisotropic magnetostriction under DC bias based on an optimized BP neural network," *IEEE Trans. Magn.*, vol. 56, no. 3, pp. 1–4, Mar. 2020.

[24] M. Rossi and J. Le Besnerais, "Vibration reduction of inductors under magnetostrictive and Maxwell forces excitation," *IEEE Trans. Magn.*, vol. 51, no. 12, pp. 1–6, Dec. 2015.

[25] M. Javorski, J. Slavic, and M. Boltezar, "Frequency characteristics of magnetostriction in electrical steel related to the structural vibrations," *IEEE Trans. Magn.*, vol. 48, no. 12, pp. 4727–4734, Dec. 2012.

[26] P. Zhang and L. Li, "Vibration properties of two-stage magnetic-valve controllable reactor," *IEEE Trans. Magn.*, vol. 54, no. 3, pp. 1–4, Mar. 2018.

[27] I. C. Nlebedim, J. E. Snyder, A. J. Moses, and D. C. Jiles, "Anisotropy and magnetostriction in non-stoichiometric cobalt ferrite," *IEEE Trans. Magn.*, vol. 48, no. 11, pp. 3084–3087, Nov. 2012.

[28] D. Chen, B. Hou, Z. Feng, and B. Bai, "Study of magnetostriction influence of electrical sheet steel under different DC biases," *IEEE Trans. Magn.*, vol. 55, no. 2, pp. 1–5, Feb. 2019.

[29] L. Chen, T. Ben, H. Zhao, C. Fang, and Y. Wang, "Characterization of magnetic properties of nanocrystalline alloys under rotational magnetization," *AIP Adv.*, vol. 9, no. 3, Mar. 2019, Art. no. 035316.

[30] (2020). *Electrical Steel Sheets JFE G-Core, JFE N-Core*. [Online]. Available: https://www.jfe-steel.co.jp

TONG BEN (Member, IEEE) was born in Hebei, China, in 1991. She received the Ph.D. degree in electrical engineering from the Hebei University of Technology, Tianjin, China, in 2018. She is currently working as a Lecturer at the College of Electrical Engineering and New Energy, China Three Gorges University. Her research interests include the magnetostriction effect modeling of soft magnetic materials and electromagnetic stress simulation of transformer and motor.

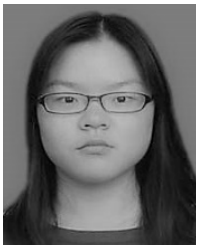

FANGYUAN CHEN was born in Hubei, China, in 1995. She received the B.E. degree in electrical engineering and automation from the Wenhua College, Wuhan, China, in 2018. She is currently pursuing the M.S. degree with China Three Gorges University, Yichang, China. Her research interest includes modeling of magnetostriction of electrical steel sheets.

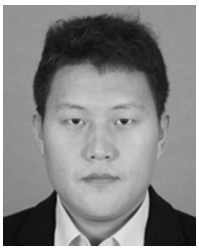

LONG CHEN (Member, IEEE) was born in Hebei, China, in 1989. He received the B.E. degree from the Hebei Normal University of Science and Technology, Qinhuangdao, China, in 2012, and the Ph.D. degree in electrical engineering from the Hebei University of Technology, Tianjin, China, in 2018. Since 2018, he has been a Lecturer with the College of Electrical Engineering and New Energy, China Three Gorges University. His research interests include measuring the magnetic properties of soft magnetic materials and hysteresis modeling.

AHMED ABU-SIADA (Senior Member, IEEE) received the B.Sc. and M.Sc. degrees in electrical engineering from Ain Shams University, Egypt, in 1998, and the Ph.D. degree in electrical engineering from Curtin University, Australia, in 2004. He is currently an Associate Professor and the Lead of the Electrical and Computer Engineering Discipline, Curtin University. His research interests include power electronics, power system stability, condition monitoring, and power quality. He is the Vice-Chair of the IEEE Computation Intelligence Society and the WA Chapter. He is the Editor-in-Chief of the *International Journal of Electrical and Electronic Engineering & Telecommunications* and a regular Reviewer of various IEEE TRANSACTIONS.

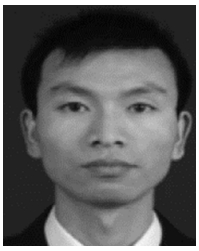

LIBING JING (Associate Member, IEEE) was born in Henan, China, in 1982. He received the Ph.D. degree in power electronics and power drive from Shanghai University, in 2013. From 2016 to 2018, he was a Postdoctoral Student with the Huazhong University of Science and Technology, Wuhan, China. Since 2016, he has been an Associate Professor with the College of Electrical Engineering and New Energy, China Three Gorges University. His research interest includes the analysis of electrical machines.

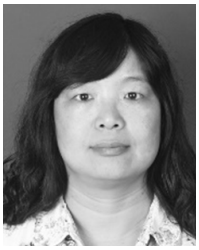

RONGGE YAN was born in Hebei, China, in 1969. She received the B.E., M.E., and Ph.D. degrees in electrical engineering from the Hebei University of Technology, Tianjin, China, in 1991, 1998, and 2003, respectively. She was a Visiting Scholar with the University of Houston, from 2010 to 2011. Since 2008, she has been a Professor with the State Key Laboratory of Reliability and Intelligence of Electrical Equipment, Hebei University of Technology. Her research interests include the electrical equipment vibration and noise reduction technology and new magnetic functional materials application research and engineering electromagnetic field numerical calculation.